Available online at www.sciencedirect.com
SCIENCE DIRECT®
Engineering Geology 70 (2003) 17–35
ENGINEERING GEOLOGY
www.elsevier.com/locate/enggeo

Dam sites in soluble rocks: a model of increasing leakage by dissolutional widening of fractures beneath a dam

Douchko Romanov[a], Franci Gabrovšek[b], Wolfgang Dreybrodt[a,*]

[a] *Karst Processes Research Group, Institute of Experimental Physics, University of Bremen, Postfach 330410 (NW1 Kufsteiner Str) D-28334 Bremen, Germany*
[b] *Karst Research Institute, Postojna, Slovenia*

Received 9 October 2001; accepted 14 January 2003

Abstract

Water flowing through narrow fissures and fractures in soluble rock, e.g. limestone and gypsum, widens these by chemical dissolution. This process, called karstification, sculptures subterranean river systems which drain most of their catchment. Close to dam sites, unnaturally high hydraulic gradients are present to drive the water impounded in the reservoir downstream through fractures reaching below the dam. Under such conditions, the natural process of karstification is accelerated to such an extent that high leakage rates may arise, which endanger the operation of the hydraulic structure. Model simulations of karstification below dams by coupling equations of dissolutional widening to hydrodynamic flow are presented. The model scenario is a dam 100 m wide in limestone or gypsum. The modelling domain is a two-dimensional slice 1 m wide directed perpendicular to the dam. It extends 375 m vertically and 750 m horizontally. The dam is located in its center. This domain is divided by fractures and fissures into blocks of $7.5 \times 7.5 \times 1$ m. The average aperture width of the fractures is 0.02 cm. We performed model runs on standard scenarios for a dam site in limestone with the height H of impounded water 150 m, a horizontal impermeable apron of width $W = 262$ m and a grouting curtain reaching down to a depth of $G = 97$ m. In a second scenario, we changed these construction features to $G = 187$ m and $W = 82$ m. To calculate widening of the fractures, well-established experimental data on the dissolution of limestone and gypsum have been used as they occur in such geochemical settings. All model runs show similar characteristic behaviour. Shortly after filling, the reservoir exhibits a small leakage of about 0.01 $m^3\ s^{-1}$, which increases steadily until a breakthrough event occurs after several decades with an abrupt increase of leakage to about 1 $m^3\ s^{-1}$ within the short time of a few years. Then, flow in the fractures becomes turbulent and the leakage increases to 10 $m^3\ s^{-1}$ in a further time span of about 10 years. The widths of the fractures are visualized in various time steps. Small channels propagate downstream and leakage rises slowly until the first channel reaches the surface downstream. Then breakthrough occurs, the laminar flow changes to turbulent and a dense net of fractures which carry flow is established.

We performed a sensitivity analysis on the dependence of breakthrough times on various parameters, determining breakthrough. These are the height of impounded water H, the depth G of grouting, the average aperture width a_0 of the fractures and the chemical parameters, which are c_{eq} the equilibrium concentration of Ca with respect to calcite and the Ca-concentration c_{in} of the inflowing water. The results show that the most critical parameter is a_0. At fracture aperture widths of 0.01 cm, breakthrough times are above 500 years. For values of $a_0 > 0.02$ cm, however, breakthrough times are within the lifetime of the structure. We have also modelled dam sites in gypsum, which exhibit similar breakthrough times. However, after

* Corresponding author. Fax: +49-421-2187318.
E-mail addresses: dromanov@physik.uni-bremen.de (D. Romanov), gabrovsek@zrc-sazu.si (F. Gabrovšek), dreybrod@physik.uni-bremen.de (W. Dreybrodt).

0013-7952/03/$ - see front matter
doi:10.1016/S0013-7952(03)00073-5

breakthrough, owing to the much larger dissolution rates of gypsum, the time until unbearable leakage is obtained, is only a few years. The modelling can be applied to complex geological settings, as phreatic cave conduits below the dam, or a complex stratigraphy with varying properties of the rock with respect to hydraulic conductivity and solubility. A few examples are given. In conclusion, our results support the assumption that increasing leakage of dam sites may be caused by dissolutional widening of fractures.

Keywords: Dam sites; Leakage; Limestone; Gypsum; Dissolution kinetics; Karst

1. Introduction

Karst is a characteristic geological feature of areas comprised of soluble rocks such as limestone, dolomite, gypsum or anhydrite. Due to the solubility of these rocks in water, karst aquifers have developed, which exhibit an extreme heterogeneity of hydraulic conductivities. Karst conduits with diameters from several millimetres up to the order of 10 m drain water from the aquifer. The storage is effected mainly in fracture systems with aperture widths from 1 mm down to the order of several tens of micrometers. These fractures and fissures also constitute most of the porosity of the aquifer, which generally amounts to a small percentage of the total rock mass. Hydraulic conductivities in these aquifers range between 10^{-8} and 10^{-5} ms^{-1} in the fracture systems, and up to 1 ms^{-1} in conduits. This extreme heterogeneity renders karst aquifers as highly complex systems with unique hydrogeological characteristics. Much of the present knowledge on the hydrogeology of karst terranes is summarized in textbooks by Ford and Williams (1989) and White (1988). Engineering aspects in karst regions are discussed in textbooks by James (1992), Breznik (1998) and Milanović (2000).

Due to their complexity, karst areas have been considered problematic as sites for the construction of large hydroprojects, including dams and reservoirs. But owing to the increasing demand for water, and the fact that about 15% of the earth's dry ice-free land is underlain by soluble rocks (Ford and Williams, 1989), a large number of dams have been constructed successfully worldwide. The present state of the art in constructing large dams has benefited from many failures in the past. For example, reservoirs could not retain water and others even never could be filled. Some reservoirs suffered from increasing water loss caused by gradual opening of joints and channels formerly filled with sediments. A list of leakages from 42 dams worldwide is given by Milanović (2000). An interesting case study on the Kar Dam has been published recently (Uromeihy, 2000).

To avoid water loss, techniques have been developed to construct grout curtains deep below the dam, with depths varying from 0.3 to 8 times the maximum water height. Even when water loss is low after the first filling of the reservoir, it may increase in time. The Great Falls Reservoir, USA showed an increase of leakage from 0.47 m^3 s^{-1} in 1926 to 6.6 m^3 s^{-1} in 1939, and to 12.7 m^3 s^{-1} in 1945, which caused a decrease of its water level by 8.1 m. (Milanović, 2000).

Karst is not static but is a highly dynamic system. Karst channels under natural conditions are created in time scales of thousands to hundred thousands of years, when hydraulic heads drive water through narrow fractures and these are widened by solution. Much understanding of details of these dynamic processes has been accumulated during the last 2 decades. These range from understanding the details of the dissolution kinetics of limestone (Dreybrodt and Eisenlohr, 2000) and gypsum (Jeschke et al., 2001), and using these to model the evolution of karst channels from initially narrow fractures. A good review on this subject is given in a recent book on the evolution of karst aquifers edited by Klimchouk et al. (2000).

Such research has raised the issue whether karstification processes could be enhanced dramatically close to dam sites, where the hydraulic gradients acting to fracture pathways leading downstream beneath the dam site can be steeper by more than two orders of magnitude compared to natural conditions.

First models on one-dimensional conduits have been worked out by James (1992), who asked the

question: could enhanced solution, especially in gypsum terranes be the cause of failures of dam sites? Published records, however, are rare and partly not easily accessible. James (1992) reports several case histories of failures due to excessive water losses, which he believes are due to dissolution of gypsum. Palmer (1988) proposed a one-dimensional model of limestone dissolution and concluded that the increasing water losses of the Great Falls Reservoir, USA result from dissolutional widening of fracture pathways, connecting the bottom of the reservoir to the valley downstream. Palmer (1988) suggested a crude estimation for hydraulic conditions under which a pathway in limestone with aperture widths in the order of about 0.01 cm would suffer dissolutional widening, leading to significant water losses. These estimations were confirmed later by Dreybrodt (1992, 1996). This work revealed the crucial parameters, determining failure of hydraulic structures. These are the aperture widths of the fractures comprising a percolating pathway, and the hydraulic ratio given by H/L^2, where H is the head (height of impounded water) and L the length of the pathway from its input in the reservoir to its output, a later spring. For hydraulic structures with $H/L^2>0.2\ m^{-1}$, water losses of about 0.5 $m^3\ s^{-1}$ could arise within 50 years for one single pathway with an initial aperture width of 10^{-2} cm and a width of 1 m. Although these models can be criticized to be not very realistic, since simple one-dimensional pre-structured pathways are highly idealistic, they still give rise to the suspicion that leakage at hydraulic structures in soluble rocks may be caused by solutional widening. First attempts on two-dimensional modelling were conducted by Dreybrodt and Siemers (2000) and Dreybrodt et al. (2001).

In this work, we present a more realistic two-dimensional model of fractured soluble rock underlying a dam site to study the evolution of the fracture widths under the action of the steep hydraulic gradients imposed by the impounded water.

2. Model structure

Fig. 1 presents an idealized dam site setting, which is not only sufficiently simple to allow numerical modelling but also sufficiently complex as an approximation of a real situation. We assume a narrow valley underlain by karstified limestone; but the slopes consist of insoluble and impermeable rocks, which extend below the surface. The dam site cutting off the valley impounds water at a height H. Its impermeable basis is of width W. Below the dam, a grouting curtain extends down to a depth G (see Fig. 2).

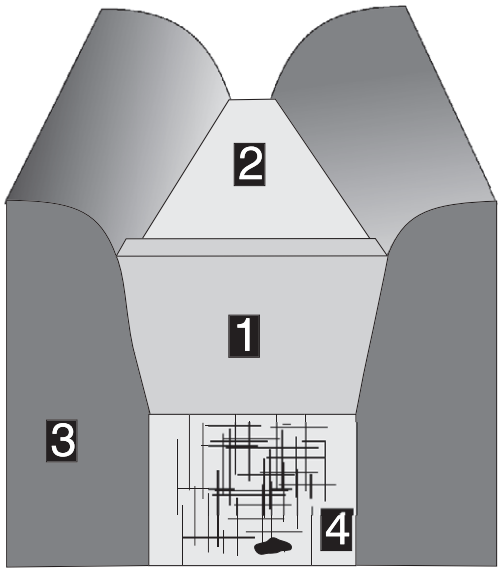

Fig. 1. Geological setting of the standard model. The dam site (1) impounding water (2) is located in a valley with impermeable slopes (3). The bottom of the valley consists of soluble rock (e.g. limestone) (4). A net of fractures dissects the limestone. Also larger voids and caves can be present.

The hydrogeological properties of the limestone are determined by the intensity of its karstification, which can be classified by three elements.

1. There is a net of primary, yet unwidened fractures and fissures, which comprise percolating pathways from the bottom of the reservoir to the valley downstream. Such a network is characterized by average spacing s of the fractures, their aperture widths a_0 and their widths b_0. One may assume two sets of fractures along the valley which are perpendicular to each other. Such a fracture system exhibits a hydraulic conductivity (Lee and Farmer, 1993),

$$K = \frac{\rho g}{12\eta}\frac{a_0^3}{s} \tag{1}$$

where ρ is the density of water, η is the viscosity and g is earth's acceleration. Assuming a spacing s of 10 m between the fractures, and average aperture widths a_0 of 1×10^{-2} cm yields a hydraulic conductivity $K = 1 \times 10^{-7}$ ms^{-1}, characteristic for a low degree of karstification.

2. In reality, not all of the fractures will be of equal aperture widths. The net of fractures can be presented as one with a log-normal statistical distribution of their aperture widths (Gale, 1987). Average widths of primary joints are about 1.5×10^{-2} cm, decreasing exponentially with depth (Lee and Farmer, 1993) to values about 8×10^{-3} cm. In rocks already karstified, these numbers may be higher. In any case, fracture aperture widths from several 10^{-2} to 3×10^{-3} cm should be considered as a reasonable range. Average spacing s of the fractures is about 5 m close to the surface, decreasing to about 10 m at depths below 50 m (Lee and Farmer, 1993). Within the primary net of narrow fractures, there may exist fractures with significantly larger aperture widths. These can form pathways connecting input and outputs. In this case, they will attract flow and dissolutional widening there will be most favourable. If such wide fractures are isolated, they still can serve as shortcuts for nearby pathways of narrow fractures.
3. Many places where dam sites have been constructed are highly karstified, exhibiting karst conduits and caves (Milanović, 2000). Therefore, intensive grouting is required in such areas. Nevertheless, karst channels may remain open, short cutting percolation pathways of fractures and thus increasing total hydraulic conductivity. In the worst case, large cave conduits well below the grouting curtain may drain water effectively to some spring.

Fig. 1 illustrates simple settings for didactic reasons. If the slopes are comprised of soluble rock, karstification can also be induced there. To model these parts, it is always possible to cut out two-dimensional slices in the area of interest as a modelling domain.

Fig. 2 presents such a two-dimensional section of the scenario shown in Fig. 1. The modelling domain is $750 \times 375 \times 1$ m, divided by fractures and fissures into blocks of $7.5 \times 7.5 \times 1$ m. To each fracture, a specific fracture aperture width is assigned. By this way, it is possible to account for the heterogeneity of the aquifer. Different lithologies of the bedrocks may cause changes in its dissolution kinetics reflected by the rate constants k_1 and k_n (cf. Eq. (2)). Therefore, these constants can also be assigned individually to each fracture. This enables one also to model regions of insoluble rock located in the modelling domain, as well as regions of highly soluble material such as gypsum. Impermeable regions resulting from grouting or by sealing the surface are modelled by omitting the corresponding fractures from the net. The influence of karstic vadose or phreatic channels which drain the area can be considered by assigning hydraulic heads h_1 between 0 and H to those nodes i where these channels are located.

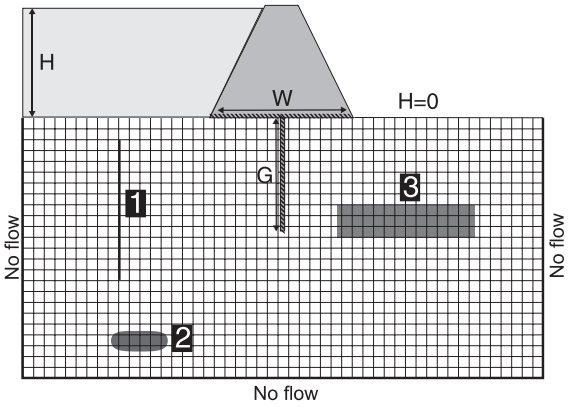

Fig. 2. Model domain of the dam site. A slice of 1-m width is taken along the valley. It is dissected by fractures and fissures into blocks of $7.5 \times 7.5 \times 1$ m^3. The domain is 750 m in horizontal extension and 375 m vertical. The bottom and the edges are impermeable (see text). The upper left-hand side is at constant head H. The dam, the sealing apron and the grouting curtain are impermeable. The right-hand side is at constant head zero. The aperture widths of the fractures separating the blocks are either uniform (standard model) or log-normally distributed (extended standard). (1) Symbolizes an open fracture, (2) a cave conduit and (3) a region of highly soluble rock (e.g. gypsum).

In summary, it is possible to model a large variety of complex geological situations, including varying stratigraphy and lithological properties of the rocks, the influence of wide fractures, e.g. faults and the existence of open isolated voids, as well as vadose and phreatic caves. We will give examples of this at the

end of this paper. But for most of this work, we assume a net of narrow fractures, because by this way the basic principles of increasing leakage can be seen most easily.

In contrast to the structure of the underlying aquifer, the boundary conditions of the hydraulic structure are most simple. At the top of the domain head is constant to the height H of the impounded water at the left-hand side of the dam, and at its right hand side, downstream head is at zero. The dam is assumed to be impermeable. This is also the case for its sealing apron of width W and the grouting curtain extending to depth G.

The bottom of the domain is assumed to be impermeable. Even in the case where the limestone reaches much deeper than the depth modelled (375 m), its intensity of karstification decreases exponentially with depth (Milanović, 1981, 2000), such that at depths of more than 400 m, the permeability of the rock becomes very low.

A problem arises to define the boundary conditions at the right- and left-hand sides of the domain, when the limestone extends vastly over the modelling domain. In that case, it is not appropriate to define these boundaries as impermeable. On the other hand, extending the modelling domain over kilometres from the dam is prevented by computational limits. As an approach, we define the boundaries as impermeable, but increase the width of the modelling domain to estimate the influence of "wrong" boundary conditions to the modelling results. If no influence to the result is found, the boundary conditions can be regarded as correct. This will be discussed later. Although the modelling program offers a wide variety to model complex geological situations, we will restrict to simple cases from which the principles of leakage evolution become obvious more easily. Extension to more complex situations such as formation of leakage from the bottom of the lake to caves located below, etc. can easily be incorporated to each specific case and an example is given later.

3. Dissolution kinetics of limestone and gypsum

The dissolution rates R of limestone and gypsum during water–rock interaction in laminar or turbulent flow have been intensively investigated. They can be described (Eisenlohr et al., 1999) by a rate law

$$R_1 = k_1(1 - c/c_{eq}) \text{ for } c \le c_s$$

$$R_n = k_n(1 - c/c_{eq})^n \text{ for } c \ge c_s \quad (2)$$

where c is the concentration of Ca in the water and c_{eq} its equilibrium concentration with respect to calcite or gypsum, respectively. c_s is a switch concentration, where the dissolution rates (mol cm^{-2} s^{-1}) switch from a linear rate law to a non-linear one with order n. The values of c_s, k_n and n are characteristic for the mineral because they are entirely dependent on surface reactions. For limestone, k_1 is controlled by surface reaction, conversion of CO_2 and diffusive mass transport of the reacting species towards and away from the mineral surface. Therefore, this value depends on the aperture width of the fracture, where solution flows and on its conditions of flow. Details on the dissolution kinetics of limestone are given by Buhmann and Dreybrodt (1985a,b), Dreybrodt (1988), Dreybrodt and Buhmann (1991), Liu and Dreybrodt (1997), Dreybrodt et al. (1996), Svensson and Dreybrodt (1992), Eisenlohr et al. (1999) and Dreybrodt and Eisenlohr (2000). The dissolution rates of gypsum have been determined by Jeschke et al. (2001).

It should be pointed out here that the switch to non-linear kinetics is of utmost importance in the evolution of the natural hydraulic conductivity of large-scale karst aquifers, both in limestone and gypsum. If the dissolution rates were entirely linear, i.e. $c_s = c_{eq}$, they would drop exponentially with distance when water flows along narrow fractures, such that after the short distance of only several 10 m, they would decay by about ten orders of magnitude (Dreybrodt and Gabrovšek, 2000; Gabrovšek, 2000). Therefore, under the action of solely linear kinetics, widening of fractures is active only close to their entrance. For percolating pathways much longer than this entrance region, the exit remains unaffected and flow rates change a little. For dissolution under the action of non-linear kinetics, the situation is entirely different. The rates now drop by a hyperbolical decay, such that even after a distance of thousands of meters, a small but sufficient dissolutional widening is operative and activates a positive feedback loop. Increasing width at the exit of

a fracture causes increasing dissolutional widening and vice versa. Therefore, flow rates through the fracture first increase slowly, but then suddenly are enhanced dramatically. After this event, called breakthrough, turbulent flow sets in, and due to the large amount of water flowing through the widened conduits, the calcium concentration drops and dissolutional widening is even along the fracture at about 0.5 mm year^{-1} in limestone (Dreybrodt, 1988; Dreybrodt and Eisenlohr, 2000), and about 10 cm year^{-1} for gypsum (Jeschke et al., 2001). The latter was also observed on a retreating gypsum cliff in nature (James, 1992).

4. Calculation of network evolution

In a first step, flow through all fractures must be calculated. Mass conservation at each node i yields the equation

$$\sum_j Q_{ij} + Q_i = 0 \tag{3}$$

where Q_{ij} is the flow between node i and nearest neighbour node j. Q_i is the direct supply of water into node i.

If the flow in the fracture (i,j) connecting nodes i and j is laminar, one has to employ Hagen–Poiseuille's law

$$Q_{ij} = \frac{\rho g a_{ij}^3 b}{12\eta L_{ij}}(H_i - H_j) = \frac{H_i - H_j}{k_{ij}^{\mathrm{lam}}} \tag{4}$$

where a_{ij} is the aperture width of the fracture (i,j) and L_{ij} its length. H_i and H_j are the hydraulic heads at nodes i and j, respectively, b is the width of 1 m common to all fractures and k_{ij}^{lam} is the hydraulic of fracture (i,j). Note that the direction of flow is given by the sign of $H_i - H_j$.

If flow is turbulent, one has to use the Darcy–Weisbach equation

$$Q_{ij} = \sqrt{\frac{2gA_{ij}^2 D_{ij}}{L_{ij} f_{ij}} |H_i - H_j|}\,\frac{H_i - H_j}{|H_i - H_j|} = \frac{H_i - H_j}{k_{ij}^{\mathrm{turb}}} \tag{5}$$

where A_{ij} is the cross-sectional area of the fracture and $D_{ij} = 2a_{ij}b/(a_{ij}+b)$ is the wetted hydraulic diameter. k_{ij}^{turb} is the hydraulic resistance of fracture (i,j) in turbulent flow. The friction factor f_{ij} is given by the Colebrook–White equation

$$\frac{1}{\sqrt{f_{ij}}} = 1.14 - 2\log_{10}\left(\frac{r_{ij}}{D_{ij}} + \frac{9.35}{Re_{ij}\sqrt{f_{ij}}}\right) \tag{6}$$

r_{ij} is the roughness of the conduit wall in cm which is taken as 2% of the conduit's aperture width, Re_{ij} the Reynolds number, ρ is the density of water, η its viscosity and g earth's acceleration. Flow is assumed as turbulent for Re>3000.

Calculation of flow rates is initiated by assuming laminar flow everywhere. The resulting system of linear equations is solved by preconditioned Conjugate Gradients method for sparse matrices (Press et al., 1992; Steward and Leyk, 1994). Then for each fracture, Re_{ij} is checked for turbulence. As turbulence is detected, the system of equations becomes nonlinear and is solved by Newton–Raphson iteration. For fractures which become turbulent, the previous value of k_{ij}^{lam} is used as the initial approximation.

Once flow Q is known in the initial net, dissolutional widening is calculated in each fracture. By use of mass balance, one obtains a differential equation for the concentration c of dissolved calcium along this fracture. For simplicity in the following equation, we omit the indices i,j.

$$R(c(x))P(x)\mathrm{d}x = Q\mathrm{d}c \tag{7}$$

x is the distance along the fracture from input node i to output node j. $R(c(x))$ are the dissolution rates along x and $P(x)$ is the perimeter changing with distance x. Once $c(x)$ is known along the fracture, widening during time step Δt is obtained by

$$a(x, t+\Delta t) = a(x,t) + 2\gamma R(c(x,t))\Delta t \tag{8}$$

where γ is a conversion factor converting from dissolution rates in mol cm^{-2} s^{-1} to retreat of bedrock in cm year^{-1} ($\gamma = 1.17\times10^9$ for limestone and $\gamma = 1.72\times10^9$ for gypsum). Details are given elsewhere (Dreybrodt,1996; Gabrovšek, 2000).

It should be noted here that in all calculations, $a(x,t)$ remains practically constant along each fracture, such that Eqs. (4), (5) and (6) can be applied. After each time-step flow is calculated, whereby as initial guess for turbulent tubes, their k_{ij}^{turb} and H_i and H_j from the previous time-step are used.

To solve Eqs. (7) and (8) in two-dimensional networks, it is necessary to know the concentrations of the inflowing solutions at each node. In the model presented here, the following procedure is used.

Start with the node at highest hydraulic head, where the input concentration is known. Search for the fractures which drain solutions away from this node. Apply the transport-dissolution procedure to these fractures (Eq. (7)) to obtain the outflowing concentrations. Go to the node which follows in the head sequence. Search for fractures draining solutions into this node and calculate the concentration at the intersection of these fractures by complete mixing. Use this as input concentration for the fractures leading flow away. Continue downward in the head sequence by the same procedure until all nodes are completed.

When flow is laminar, the dissolution rates R are given by Eq. (2), whereby at each fracture, these rates are compared to diffusional rates given by

$$R_D = \frac{D}{a} c_{eq}(1 - c/c_{eq}) \tag{9}$$

where D is the coefficient of diffusion for Ca^{2+} ions (1×10^{-5} cm^2 s^{-1}). The smaller rates are used.

When flow becomes turbulent, a diffusion boundary layer separates the rock surface from the turbulent bulk of the solution. Its thickness ε is related to the Sherwood number by (Beek and Muttzall, 1975)

$$\mathrm{Sh} = \frac{a}{\varepsilon} \tag{10}$$

which is obtained (Incropera and Dewitt, 1996) by

$$\mathrm{Sh} = \frac{(f/8)(Re - 1000)\mathrm{Sc}}{1 + 12.7(f/8)^{1/2}(\mathrm{Sc}^{2/3} - 1)} \tag{11}$$

where f is the friction factor given by Eq. (6), and Sc is the Schmidt number, which is 10^3 for water.

The dependence of the dissolution rates R for limestone on thickness ε has been investigated by Dreybrodt and Buhmann (1991) and Liu and Dreybrodt (1997). It turns out that for ε>0.01 cm, the rates become independent on ε with $k_1 = 4 \times 10^{-11}$ mol cm^{-2} s^{-1}. After breakthrough, the calcium concentration becomes low and only first order kinetics is active. Mostly ε>0.01 cm.

For gypsum, the effective transport constant k_{gyp} is obtained by mixed kinetics (Jeschke et al., 2001) as

$$k_{gyp} = \frac{k_1 \frac{Dc_{eq}}{\varepsilon}}{k_1 + \frac{Dc_{eq}}{\varepsilon}} \tag{12}$$

The dissolution rate law for gypsum is thus given by $R_{gyp} = k_{gyp}(1 - c/c_{eq})$ for $c < c_s$ and by Eq. (2) for

Table 1
Model parameters

Description	Symbol	Unit	Numerical values
Network parameters			
Initial fracture aperture width	a_0	cm	0.02
Fracture width	b	cm	100
Fracture length	L	cm	750
Domain dimension		m	750×375
Parameters of dam site			
Hydraulic head	H	m	150
Grouting depth	G	m	97 (A), 187 (B)
Apron width	W	m	262 (A), 82 (B)
Limestone: chemical parameters			
Order of non-linear kinetics	n		4
Non-linear kinetics constant	k_n	mol cm^{-2} s^{-1}	4×10^{-8}
Concentration of calcium	c	mol cm^{-3}	$c_{in} < c < c_{eq}$
Initial concentration	c_{in}	mol cm^{-3}	0
Switch concentration	c_s	mol cm^{-3}	0.9 c_{eq}
Equilibrium concentration	c_{eq}	mol cm^{-3}	2×10^{-6}
Dynamic viscosity of the solution	μ	g cm^{-1} s^{-1}	0.01
Density of the solution	ρ	g cm^{-3}	1
Gypsum: chemical parameters			
Order of non-linear kinetics	n		4.5
Non-linear kinetics constant	k_n	mol cm^{-2} s^{-1}	3×10^{-3}
Concentration of calcium	c	mol cm^{-3}	$c_{in} < c < c_{eq}$
Initial concentration	c_{in}	mol cm^{-3}	0
Switch concentration	c_s	mol cm^{-3}	0.95 c_{eq}
Equilibrium concentration	c_{eq}	mol cm^{-3}	15.4×10^{-6}
Dynamic viscosity of the solution	μ	g cm^{-1} s^{-1}	0.01
Density of the solution	ρ	g cm^{-3}	1

$c > c_s$. All constants used in the model are listed in Table 1.

5. Results

5.1. One dimensional single fracture

To understand later results on the evolution of networks, we first, for didactical reasons, consider the evolution of a single isolated fracture with length L, initial aperture width a_0 and width $b = 1$ m, with a hydraulic head H at its input and zero at its output ($a_0 = 0.02$ cm, $H = 150$ m, $L = 330$ m). The chemical parameters are those listed in Table 1. The length of this fracture has been chosen approximately $L = W + 2G$ and is close to the shortest pathway through fractures from the left-hand side input of the dam site to its output downstream. The evolution of leakage through such an isolated fracture can be regarded as a first crude approximation to the problem (James, 1992; Dreybrodt, 1992, 1996). Fig. 3 shows the results of the computer run. Fig. 3a illustrates for various times the profiles of aperture widths shaped along the fracture by dissolutional widening of the initially plane parallel fracture. In the early phase, dissolution is only active close to the entrance and a funnel-like shape evolves there. However, due to non-linear kinetics, a slow dissolutional widening is still active at the exit. This can be seen in the later profiles. This opening at the exit enhances the flow rate through the fracture, and therefore, the funnel-like opening at the entrance propagates further downstream, and also the dissolution rates at the exit increase further. This positive feedback loop creates a breakthrough event by which in a very short time, the exit widths open up dramatically fast and so do the flow rates, shown by Fig. 3b. After breakthrough, flow becomes turbulent (dashed lines). The flow rates are so high now that the concentration of calcium becomes close to zero and dissolution rates are even along the fracture. Therefore, as time proceeds, the funnel-like shape becomes smoothed out.

This evolution is accompanied by a varying head distribution along the fracture depicted by Fig. 3c. Initially, when the fracture is plane parallel, the head drops linearly from the input to the output. But with increasing width of the entrance region, the flow

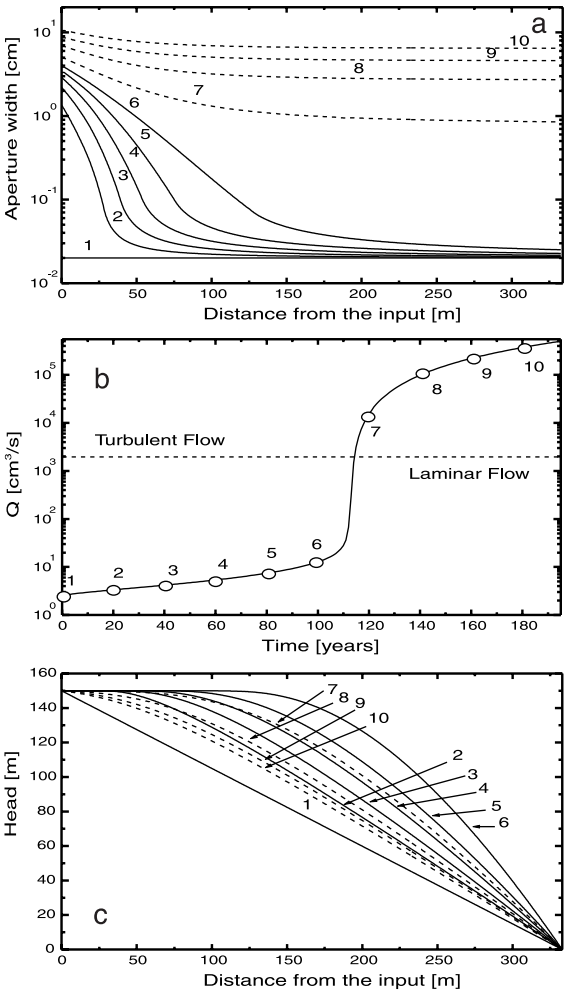

Fig. 3. Evolution of a single conduit: (a) profiles of aperture widths along the fracture, as they evolve in time. Full lines depict laminar flow. After breakthrough flow becomes turbulent (dashed lines). The numbers on the curves indicate times. (b) Flow rate through the fracture as a function time. The circles indicate the times in (a). (c) Distribution of hydraulic heads along the fractures for the times indicated in (b).

resistance of this part of the fracture becomes low and consequently the drop of head also. By this way, the head in this opened region becomes very close to the input head and the head drop is concentrated to the yet unwidened exit part of the fracture, where high gradients occur. After breakthrough, the fracture profiles become more even, and within a very short time, the heads are redistributed more evenly along

the fracture. It is important to note that this redistribution of heads during the evolution of widening fractures is an intrinsic property of karst aquifer evolution, and as will be shown in the next section is also characteristic for the evolution in fracture networks.

5.2. Standard scenarios in limestone terranes

We first treat a very simple scenario A which is shown by Fig. 2. The model domain is 750 m horizontally and 375 m in depth. The dam is located in the middle position of an impermeable horizontal sealing apron at the base extending in both directions to a width $W=262$ m. An impervious grouting curtain below the dam reaches to a depth $G=97$ m. The reservoir at the left hand side of the dam provides a hydraulic head $H=150$ m. At the right-hand side, the head is constant at zero. The dam, the sealing apron and the grouting are assumed as impermeable. The fracture system in the rock is modelled by two sets of parallel fractures perpendicular to each other with spacing of 7.5 m each. Aperture width of all fractures is 0.02 cm and their width is 100 cm. This divides the domain into a net of 100×50 elements. We assume that the concentration of Ca in the impounded water is low. Therefore, we assume $c_{in}=0$. c_{eq} is set to 2E-6 mol cm^{-3}. The dissolution constants k_1, k_n and n have been taken typical for limestone (Eisenlohr et al., 1999). All parameters for this scenario are listed in Table 1.

The network of fractures now offers various quasi one-dimensional pathways connecting inputs and outputs. Dissolutional widening along these proceeds similar as in the one-dimensional fracture. Therefore, wider channels start to propagate down head and the one with the most favourable conditions, e.g. shortest distance from input to output, will break through first.

This evolution is shown by Fig. 4a–f. After 31 years, such a channel has propagated vertically downwards close to the left rim of the sealing apron and parallel to the grouting. At its upper end, the aperture width is about 2 cm, and it is about 0.2 cm at a depth of 100 m. Fig. 4 also shows the head distribution depicted by head lines (see the bar code in Fig. 4). At the onset of the simulations, the head lines are evenly distributed as one expects for an aquifer with constant hydraulic conductivity (not shown here). After 31 years, however, this even distribution is distorted since due to the low resistance of the channel, the head at its tip is high and close to the pressure at the bottom of the reservoir. Therefore, similar as in the one-dimensional fracture (see Fig. 3c), the head drop proceeds along the yet unwidened part of the aquifer. After 71 years, the vertical channel has propagated further downwards. But now, dissolutional widening also creates two competitive horizontal channels extending below the grouting (Fig. 4b). After 88 years, they have extended further and vertical channels start to grow upwards (Fig. 4c). In all cases, due to the low resistance of flow, the hydraulic head at the tips of the channels is high, as can be visualized by the isolines and the drop of head occurs in the yet unwidened part of the aquifer. This behaviour reflects the head distribution of the single one-dimensional channel. After breakthrough at 91 years (Fig. 4d), the profiles along the pathways become leveled out and therefore the isolines become more evenly distributed as shown by Fig. 4e and f. Furthermore, flow has become turbulent, and under these conditions, dissolution has created a vast net of widened channels. During the entire evolution of the aquifer below, the dam horizontal and vertical fractures can be widened by differing amounts, and therefore, the average hydraulic conductivity becomes anisotropic. As a consequence, flow lines and head isolines are no longer vertical to each other.

Fig. 5 illustrates the total leakage of the dam as it evolves in time. This leakage is the sum of the flow rates in all fractures which have their output at $H=0$ downstream (cf. Eqs. (4) and (5)). We have also visualized as dashed curves Q_{max}. This is the flow in the fracture which carries the largest flow rate in comparison to all the others.

After a slow increase for a long time, the flow rates are enhanced dramatically at 87 years (see Fig. 4c). The time when this happens has been termed breakthrough time (Dreybrodt, 1990, 1996). This behaviour has been found also in models of natural karst evolution (Palmer, 1991; Dreybrodt, 1990, 1996; Dreybrodt and Gabrovšek, 2000; Dreybrodt and Siemers, 2000; Gabrovšek, 2000; Groves and Howard, 1994; Howard and Groves, 1995; Siemers

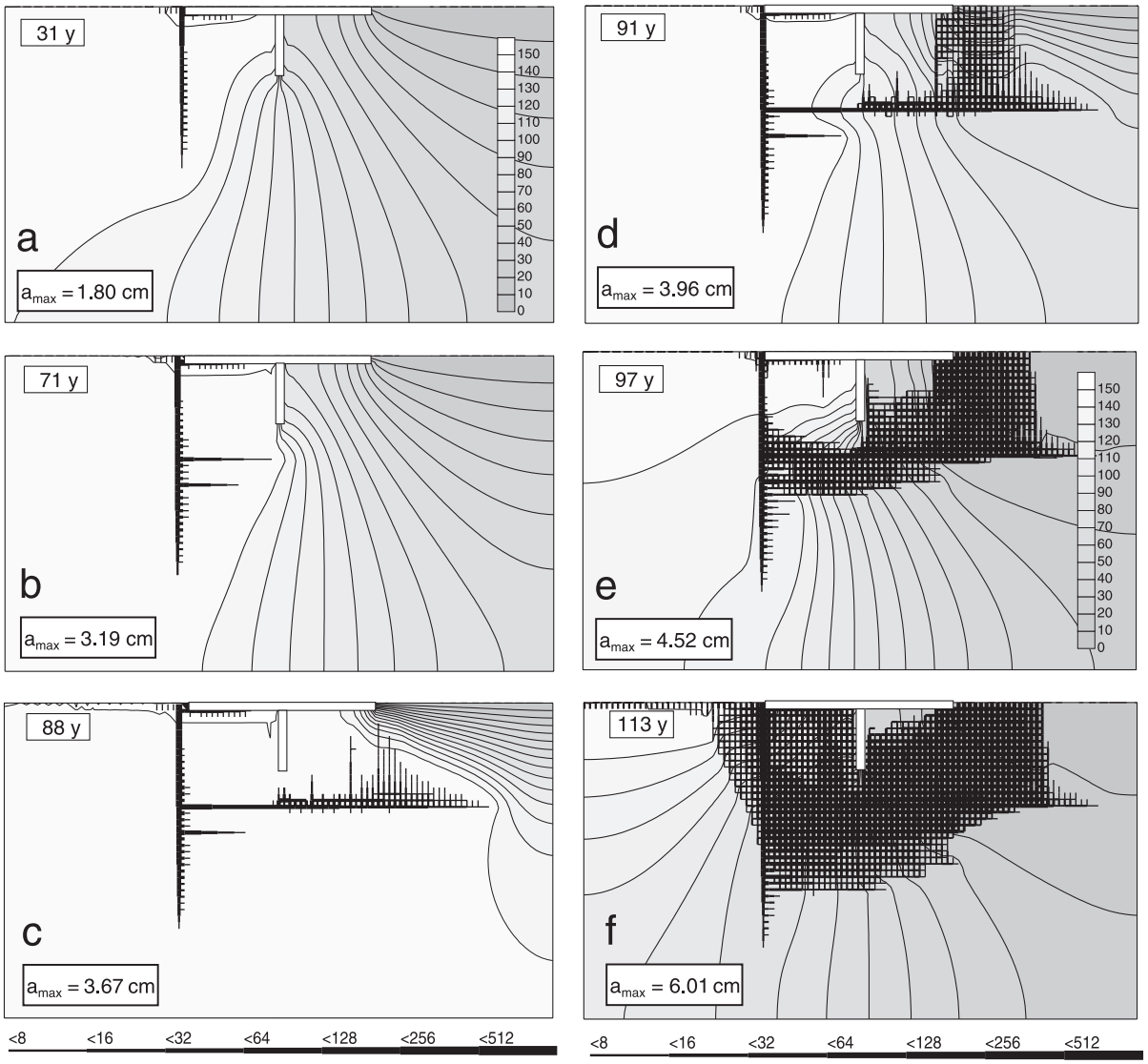

Fig. 4. Evolution of fracture widths (standard model A) with initially uniform fractures of aperture widths $a_0 = 0.02$ cm. (a) After 31 years, a shaft with maximum width of 1.8 cm has penetrated downwards. (b) After further growth downwards, horizontal channels extend below the grouting (71 years). (c) A series of conduits grows upwards and finally reaches the surface at breakthrough time after 88 years. (d–f) After breakthrough, flow becomes turbulent and a dense net of channels is created. The isolines depict the distribution of hydraulic heads in steps of 10 m. Prior to breakthrough, due to the penetrating channels, the hydraulic line of 140 m is close to the tips of the evolving conduits. The hydraulic gradient from those tips to the surface is steep and increases with time. After breakthrough, heads are redistributed with an almost even hydraulic gradient from the bottom of the reservoir to the surface downstream. The widths of the fractures in units of a_0 are given by the bar code below in units of a_0. Only fractures with width $a > 8\ a_0$ are shown. The insets show the maximum aperture widths, which are located at the input.

and Dreybrodt, 1998). Note that the flow rates are given per meter of the width of the dam, since the width of the fractures has been taken as 100 cm. Therefore, for a dam with horizontal extension of hundred meters, an initial leakage of 6 l s^{-1} is negligible. But it increases by about two orders of

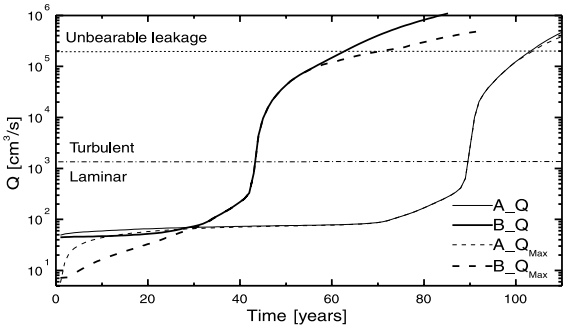

Fig. 5. Evolution of flow rates in time for standard model A (see Fig. 4) and standard model B (see Fig. 6). Q denotes the total leakage per 1-m width of the dam site. Q_{max} is the flow rate in that fracture which carries maximal flow with respect to all the other ones. In the beginning, Q_{max} is lower than Q, indicating that the flow is shared between many output fractures. Q increases slowly, whereas Q_{max} approaches Q after 10 years. This shows that the leakage concentrates to one percolating pathway with one or only few output fractures. At breakthrough, Q and Q_{max} are almost identical. After breakthrough, a dense net of flow paths arises distributing flow to many output points and consequently Q_{max} drops below Q. The dashed–dotted lines separate the regions of laminar and turbulent flow. The dotted line indicates the limit of unacceptable leakage.

magnitude at breakthrough when turbulent flow sets in. After breakthrough, under turbulent flow conditions, leakage rates increase more steadily until they reach a value of 10^5 cm^3 s^{-1}. This amounts to the unbearable leakage of 20 m^3 s^{-1}. Due to the rapidly increasing flow, the calcium concentration drops to low values, less than 0.1 c_{eq}, in all those conduits carrying turbulent flow. As a consequence, dissolutional widening increases steeply to its maximum value. This is 0.05 cm year^{-1} for limestone and about 10 cm year^{-1} for gypsum.

Shortly after breakthrough, the aperture widths still decrease downstream along the leading conduits. Therefore, the hydraulic head distribution remains steeper downstream, but differs significantly as can be seen from Fig. 4d from that shortly before breakthrough. As time passes, almost equal dissolution rates along the conduits level out the widths profiles and the head distribution becomes more even, as depicted by Fig. 4e–f.

Once a leading fracture has experienced breakthrough, the redistribution of heads injects water with low Ca concentration into yet narrow neighbouring fractures and creates a new loop of turbulent flow. Therefore, a net of loops grows along the leading conduits and the region of turbulent flow expands. In detail, the mechanism of that growth in its interaction between local redistribution of heads and dissolutional widening is quite complex. For gypsum, these mechanisms are similar in principle, but owing to the extremely high dissolution rates, the time scale for widening of the leading conduits is so short ($\approx$ 1 year, see also Figs. 9 and 10) that no time is left for the development of further turbulent loops.

A second simple scenario B of leakage evolution is shown by Fig. 6. Here the grouting curtain reaches to a depth of $G = 187$ m, but the sealing width has been reduced to $W = 82$ m, such that the sum of twice the grouting depth G and sealing width W is the same as in Fig. 4.

Fig. 6a shows the situation after 26 years. A vertical channel has extended close to the grouting depth. Widening of the fractures is restricted close to this channel. After 33 years, the vertical channel has penetrated deeper (Fig. 6b). The pressure lines show that at that time, flow is directed more towards the region close below the grouting curtain. Consequently, horizontal channels start to grow. After 43 years, a main channel has penetrated below the grouting. It has divided into a vertical channel which has reached the surface and a horizontal one which has progressed further (Fig. 6c). The width of the channels which have reached the surface is about 1 mm at their exits. The evolution of leakage is shown by Fig. 5. It is obvious that breakthrough times are highly affected.

After breakthrough, when flow becomes turbulent, the Ca concentration becomes low, below 0.1 c_{eq}, along those channels which carry most of the flow, and therefore widening becomes even along them. Fig. 5 also depicts the evolution of Q_{max}, the flow in that fracture which has the largest value of flow in comparison to all the others. In the initial phase of flow evolution, Q_{max} is significantly smaller than the total leakage Q. This indicates a distribution of leakage over many fractures. Close to breakthrough, Q_{max} and Q coincide, because flow is concentrated now to only one, or very few fractures. These widen quickly during turbulent flow. Since widening is even along these conduits now, they approach profiles of almost equal widths. Therefore, the heads are redistributed evenly in contrast to the situation before

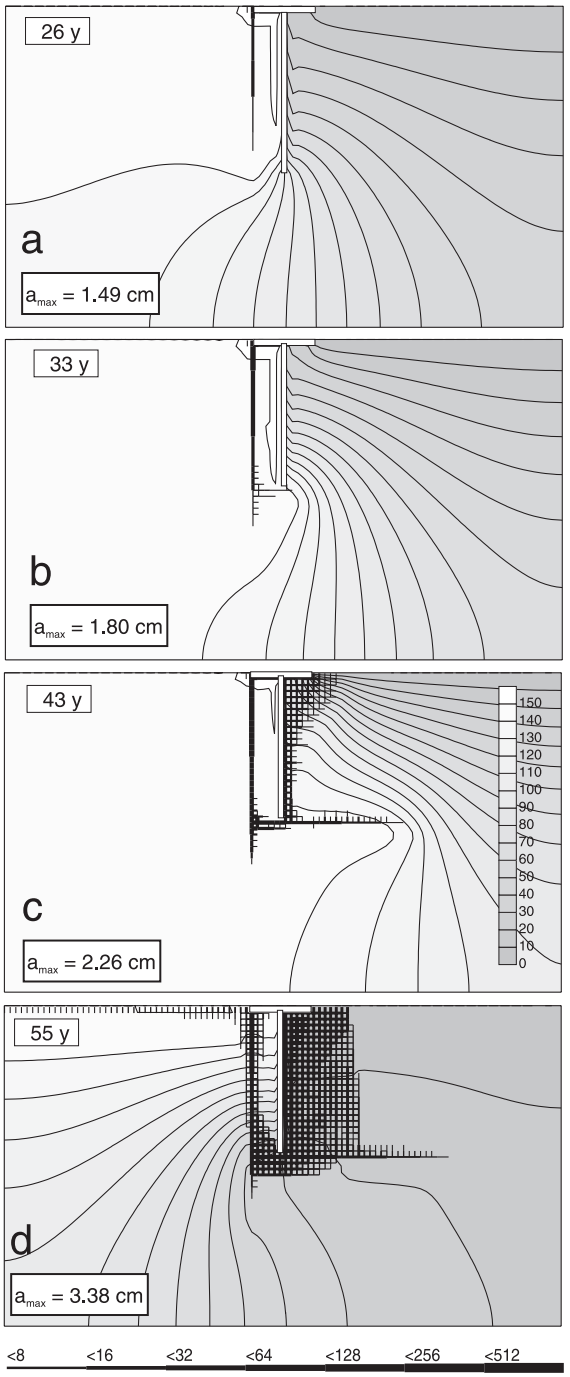

Fig. 6. Evolution of fracture widths (standard model B). Evolution is similar to standard model A (see Fig. 4). Due to the small impermeable base of the dam, the horizontal channels need only short distances to penetrate below the grouting and the breakthrough time is shorter.

breakthrough, and hydraulic gradients become almost constant in the entire aquifer (see Figs. 4e–f and 6d). Five years after breakthrough, the leading conduit has grown to about 1 cm. The increase of leakage after breakthrough for this channel can also be estimated by use of the Darcy–Weisbach equation combined with the Colebrook–White formula as $\Delta Q(t) \propto t^{3/2}$, where t is the time after breakthrough. At a hydraulic gradient of 0.4, the flow rate for a fracture of 2-cm width is 3×10^4 cm^3 s^{-1}. After further 10 years, one finds about 10^5 cm^3 s^{-1} in agreement to the data in Fig. 5. As the conduits widen further, Q_{max} departs from Q, indicating that flow becomes distributed to other conduits.

5.3. Extended standard scenarios

Fracture networks with equal aperture widths in all fractures have been chosen so far in the standard scenarios to show the principles of the evolution of karst channels below a dam site. To approach closer to nature, we have extended these standard scenarios by using statistically distributed fracture aperture widths. Laboratory work by Gale (1987) indicated a log-normal distribution of aperture widths. We have introduced such a distribution with mean value $a_0 = 0.02$ cm and $\sigma = 0.01$, where σ gives the width of the distribution.

Fig. 7 shows the evolution of karstification for the extended standard model A. Again we find a vertical channel which migrates downwards. In contrast to standard A with equal aperture widths everywhere, there is a distribution of more favourable pathways with larger average aperture widths compared to the neighbouring pathways. Therefore, diversion of the evolving channel towards the grouting wall occurs much earlier and breakthrough happens at a shorter time of 55 years compared to 90 years in the standard model A. We have performed 10 different realisations of log-normally distributed nets. Although details are different, the general behaviour is the same. Breakthrough times vary between 45 and 55 years.

Fig. 8 shows the extended standard model B also using log-normally distributed aperture widths, which behaves very similar to standard B, because pathways are close to the grouting wall. Therefore, the advantage of using more favourable pathways is lost.

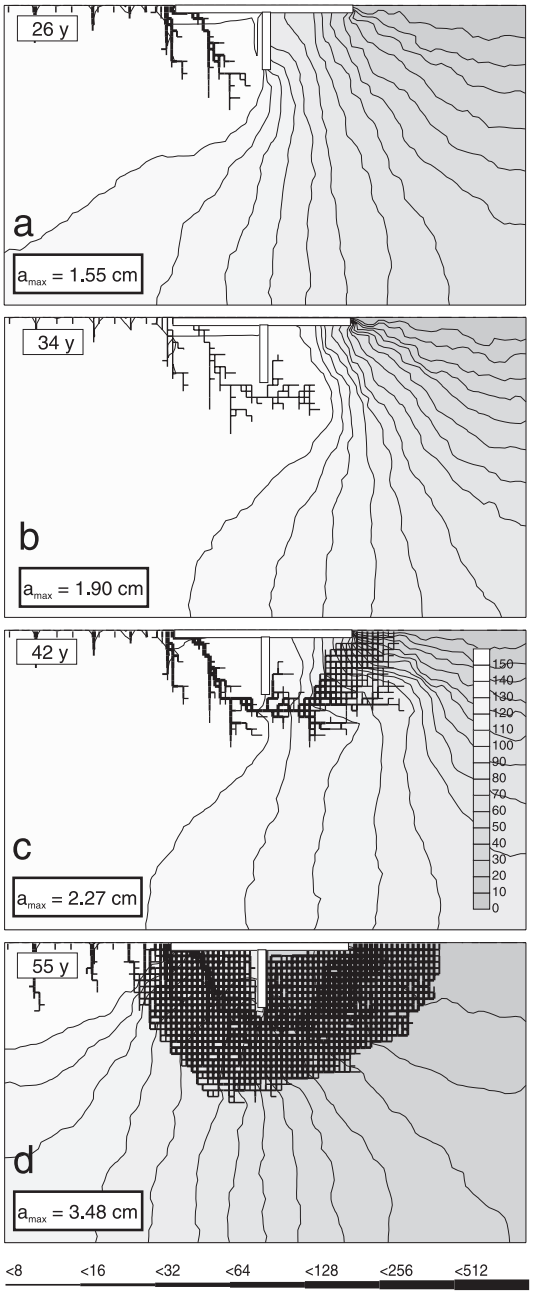

Fig. 7. Evolution of fracture widths of the extended standard model A with initially log-normal distributed fracture widths. In contrast to standard A with uniform fracture aperture, more favourable initial pathways exist and the evolution of conduits follows them, avoiding the development of a deep shaft as in Fig. 4. Therefore, breakthrough time is reduced.

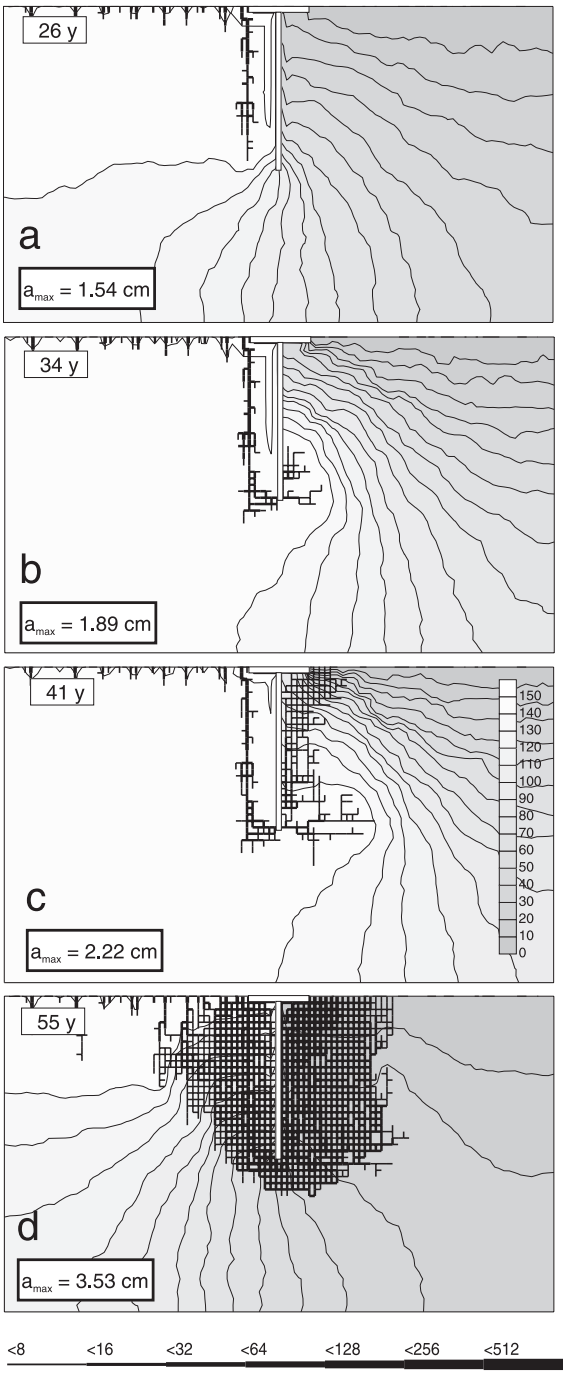

Fig. 8. Evolution of fracture widths for extended standard model B.

Fig. 9 illustrates the time dependence of Q_{max} and Q for both extended scenarios A and B.

5.4. Results for gypsum

We have also performed runs of scenarios A and B assuming gypsum as bedrock. The dissolution constants are taken from the work of Jeschke et al. (2001) and are listed in Table 1. The breakthrough times are very similar to those of limestone, since breakthrough is mainly determined by the non-linear part of the rate laws. After breakthrough due to the much higher first order dissolution rates of gypsum at about 10 cm year^{-1}, high leakage rates are created in very short times.

Fig. 10 as an example depicts the results for the extended standard model A in gypsum. Due to the much larger dissolution rates, fracture widening is restricted to only a few fractures, which evolve quickly. Breakthrough time is similar as in limestone. After breakthrough, however, flow rates increase extremely fast compared to limestone. This can be seen from Fig. 11 which depicts Q and Q_{max}.

5.5. Sensitivity analysis

The aperture widths of fractures are not very well known in nature and furthermore are statistically distributed. To gain some estimate of their influence to breakthrough time, we have varied a_0 between 0.01 up to 0.04 cm in the standard models A and B. Everything else is unchanged. We have also performed this procedure on the statistical nets of the extended standard models A and B, whereby we have also changed σ

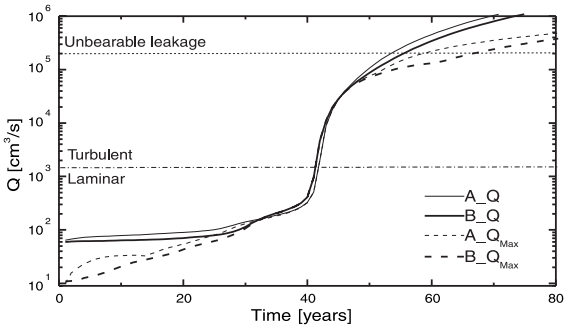

Fig. 9. Evolution of flow rates Q and Q_{max} for the extended standards A and B. The behaviour is similar as in Fig. 5.

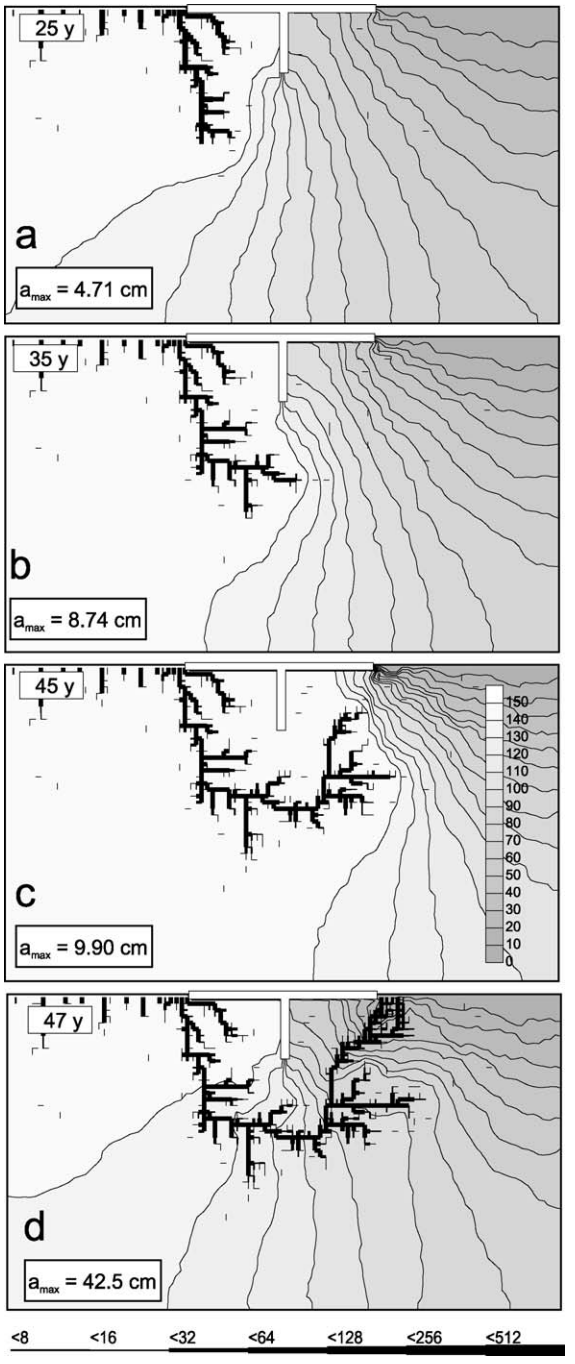

Fig. 10. Evolution of aperture widths for extended standard A in gypsum. Due to the much higher rates of widening for gypsum, the flow to the output remains restricted to mainly one prominent pathway.

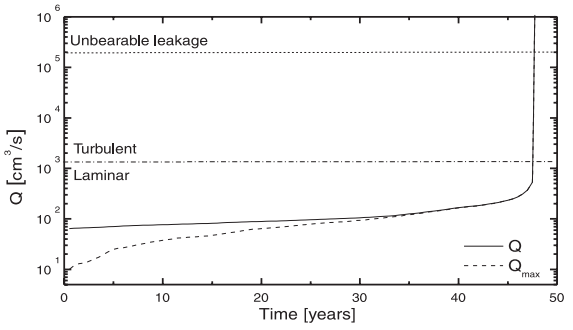

Fig. 11. Evolution of leakage Q and Q_{max} in standard A in gypsum. In contrast to limestone due to the much larger dissolutional widening rise Q is extremely steep. Q and Q_{max} coincide after breakthrough because the main flow is concentrated in a single conduit.

accordingly. Fig. 12a shows the breakthrough times in dependence on a_0 in a double logarithmic scale. Note that for fracture widths smaller 0.03 cm, the curves can be reasonably well approximated by $T_B \propto a_0^{-3.7}$. Such power laws for breakthrough times have already been found on one-dimensional conduits (Dreybrodt, 1996; Dreybrodt and Gabrovšek, 2000), and for breakthrough on two-dimensional percolation nets by Siemers and Dreybrodt (1998). For fracture widths larger than 0.03 cm, breakthrough times are reduced to values of about 10 years, and dams could be regarded as critical. On the other hand, fractures of 0.01 cm aperture widths yield breakthrough times of about 1000 years.

Another critical parameter is the height H of the impounded water. Fig. 12b depicts double-logarithmic plots for breakthrough times as a function of H. Again we find a power law $T_B \propto H^{-1.8}$ similar to what has been found earlier for single channels Dreybrodt (1996) and percolation nets (Siemers and Dreybrodt, 1998).

In the construction of dams, grouting plays a most important role. Fig. 12c illustrates the dependence of breakthrough time on the depth G of the grouting curtain. Breakthrough times increase steeply, when the grouting depth becomes larger than the height H.

In all scenarios so far, we have assumed that the water entering has not yet dissolved the soluble rock and consequently $c_{in} = 0$. To investigate what happens when the water enters with a higher concentration, we have plotted in Fig. 13a breakthrough times as a function of c_{in}/c_{eq}. For $c_{in}/c_{eq} < 0.5$ little variation is found. The closer, however, c_{in}/c_{eq} approaches saturation the higher are breakthrough times. Therefore, the saturation state of the reservoir water is a parameter of utmost importance. If water entering the fractures is close to saturation ($c/c_{eq} > 0.8$), karstification below the dam site is delayed.

A second important chemical parameter in limestone is the equilibrium concentration c_{eq} which

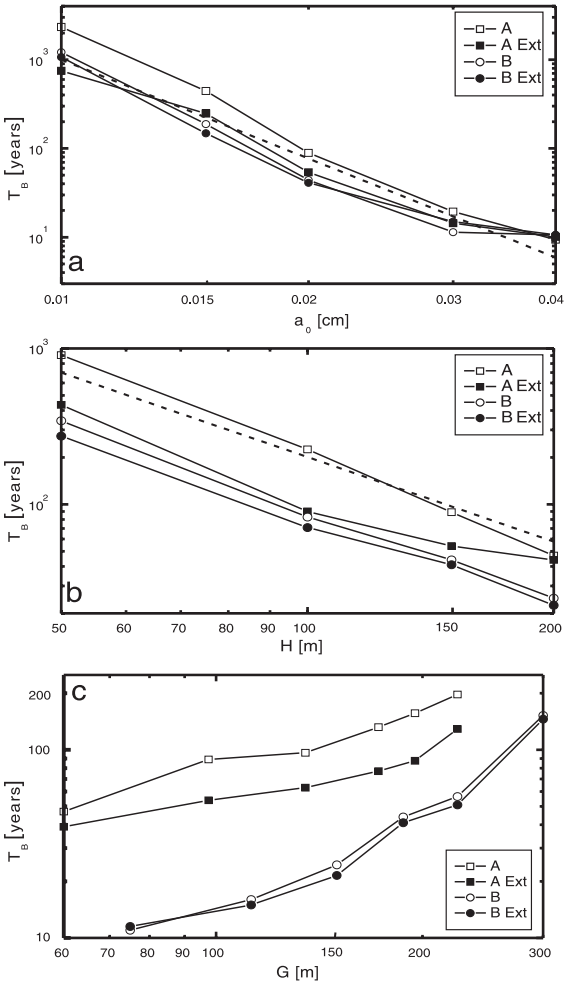

Fig. 12. Dependence of breakthrough times for standard models A (□) and B (○), and the extended standard models A (■) and B (●) in dependence on the hydrologic parameters: (a) dependence on the average initial fracture width a_0. The straight dashed line depicts the dependence $T_B \propto a_0^{-3.7}$ (see text); (b) dependence on hydraulic head. The straight dashed line depicts $T_B \propto H^{-1.8}$; (c) dependence on grouting depth.

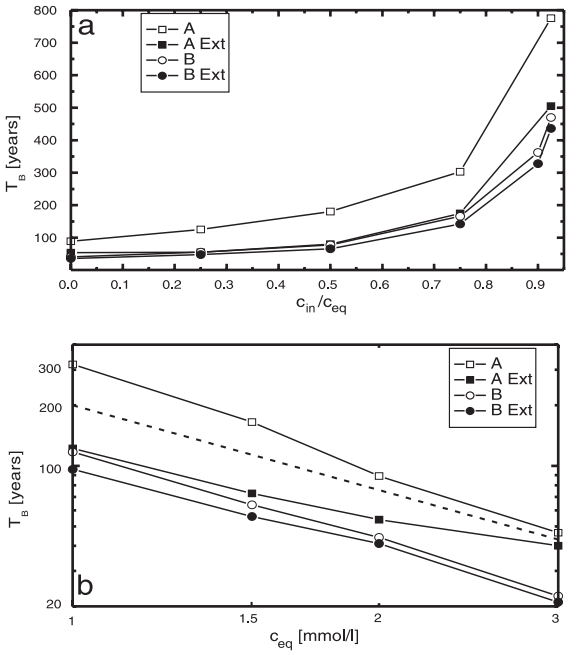

Fig. 13. Dependence of breakthrough times on chemical parameters. Symbols as in Fig. 12. (a) Dependence on the calcium concentration c_{in} of the reservoir water; (b) dependence on the equilibrium concentration with respect to calcite. The straight dashed line depicts $T_B \propto c_{eq}^{-1.4}$.

depends on the concentration of CO_2 at the bottom of the reservoir. The dependence of breakthrough times on c_{eq} is shown by Fig. 13b. Breakthrough times roughly follow a power law similar to what has been found on single tubes and percolation networks. It should be noted here that c_{eq} is the equilibrium concentration for dissolution of calcite in a system closed with respect to CO_2. It depends on the CO_2 and the calcium concentration in the reservoir water (Dreybrodt, 1996), when it enters into the fractures.

In scenarios A and B, we have assumed a domain of 750-m width and 375-m depth. As we have noted earlier, the width of the domain could be critical to our calculations because of the artificial boundary conditions (left- and right-hand sides are regarded impermeable). We have therefore extended the domain to 1500 m width, keeping the depth at 375 m. The size of the grids remained unchanged at 7.5×7.5 m^2. The breakthrough times and the channel patterns remained unaffected. This asserts that the domain of our standard scenarios is reasonable. Reducing this domain, however, by a factor of one half to a 50×50 net, with a horizontal width of 375 m, shows an increase of breakthrough times by about 30%.

To obtain some idea on the breakthrough behaviour of smaller dams, we have scaled H, G and W by a common factor f_s. In other words, we reduce the dimensions of the structure by f_s. Fig. 14 shows the breakthrough time in dependence on the scaling factor f_s. Breakthrough times decrease for all scenarios with decreasing size of the structure. At $f_s = 0.5$, breakthrough times are reduced to about one half compared to the standard scenarios. This means that especially for smaller structures comparatively deeper grouting is necessary to prevent karstification below the dam. Again, this behaviour reflects breakthrough properties of single conduits and percolation nets. Their breakthrough times follow a power law $T_B \propto (L^2/H)^{4/3}$, where L is the length of the channel (Dreybrodt, 1996; Dreybrodt and Gabrovšek, 2000). In our cases, L is close to $W + 2G$. Scaling W, G, H by a common factor f_s scales T_B by $(f_s)^{4/3}$.

So far we have considered a very simple geological setting with a net of narrow fractures solely. This corresponds to the ideal situation, where all open voids, fractures or even cave conduits have been sealed by grouting. To see the influence of a phreatic cave conduit below the dam, we have modelled such a situation. We have introduced into the extended standard model A, a phreatic cave conduit, well below the dam. This is indicated by

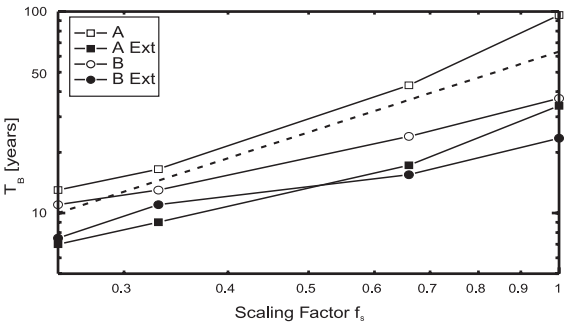

Fig. 14. Scaling law: dependence of the breakthrough time on the scaling factor f_s (see text) for standards A (□) and B (○), and the extended standards A (■) and B (●). The straight dashed line depicts the relation $T_B \propto f_s^{4/3}$.

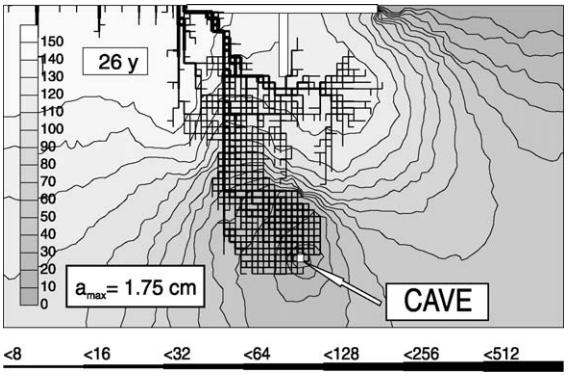

Fig. 15. Extended standard model A with a cave conduit deep below the dam site: fracture widths and head distribution at breakthrough.

the white square in Fig. 15. The boundary conditions at all fractures comprising this area are set to 0.1 m. This corresponds to a head of a phreatic cave conduit, which has its spring somewhere down stream of the dam site. Fig. 15 depicts headlines and fracture widths after 26 years. There are two competitive routes to breakthrough. One is leading below the dam and grouting to the outputs downstream with head zero. The other one is directed towards the cave conduit with similarly low head. In our scenario, this last pathway is more competitive and breakthrough into the conduit arises after 26 years, much earlier than the extended standard model A with 42 years. The evolution of total leakage is illustrated by Fig. 16.

In our standard models, we have assumed that the rock is homogeneous with respect to its dissolutional properties. We now relax this by inserting a horizontal layer of insoluble rock extending from the left-hand side boundary below the dam to the right-hand side border. Its thickness is 67.5 m. The fracture width's distribution remains unchanged, as in extended standard scenario A. Fig. 17a shows a setting, where the grouting curtain has not reached this layer and a thin layer of soluble rock remains between the grouting and the insoluble rock. It further depicts isolines of head and fracture widths distribution after breakthrough at 45 years. Breakthrough has occurred via the small soluble fringe between the tip of the grouting and the layer of insoluble rock. Head distribution and the structure of flow conduits resemble very much that of extended standard model A, depicted in Fig. 7b and c. The evolution of total leakage is depicted in Fig. 16.

A completely different behaviour results when grouting reaches into the insoluble layer as shown in Fig. 17b. Now the pathway to breakthrough below the dam is blocked. Widening of fractures occurs above the insoluble layer and also at its lower border. But breakthrough is prevented because all the water leaking below the dam must pass through the insoluble layer, where fractures are not enlarged. Therefore, this layer limits flow rates, even when the permeability in the rock above increases significantly. This is also shown by the evolution of flow rates shown in Fig. 16.

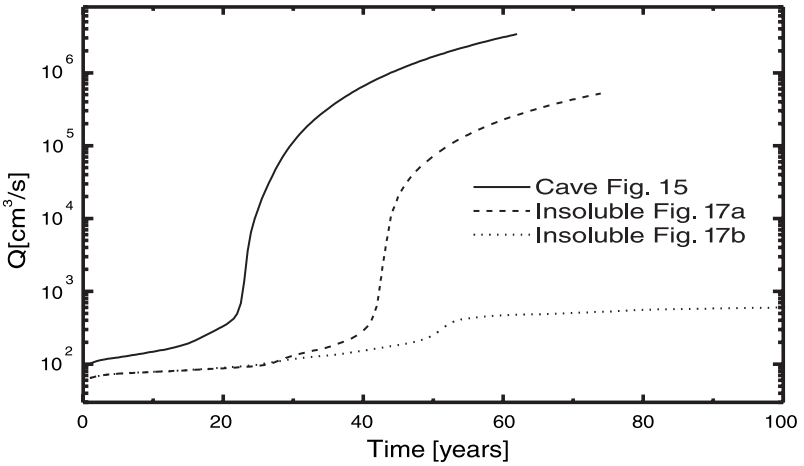

Fig. 16. Evolution of total leakage in time for the geological settings in Figs. 15 and 17a and b.

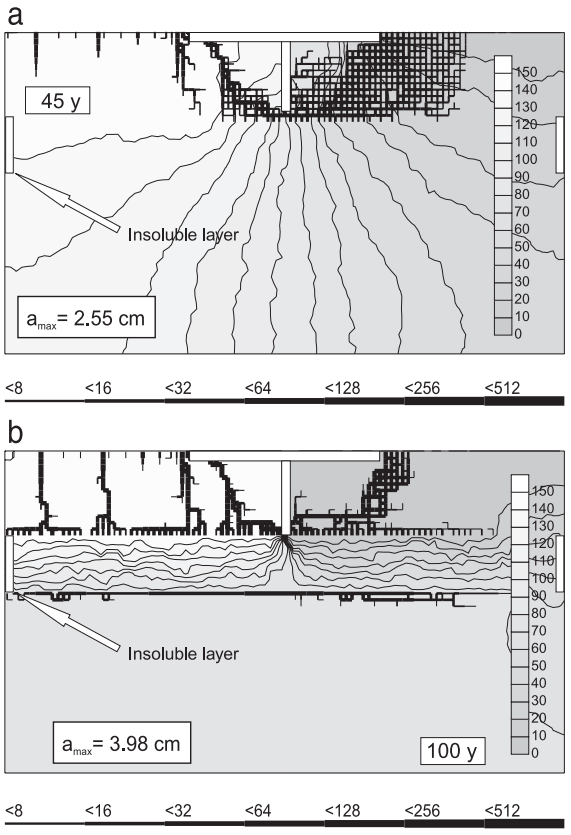

Fig. 17. Extended standard model A with an insoluble layer of rock, extending horizontally between white vertical bars at the rims. (a) The grouting curtain does not reach into the insoluble layer. (b) The grouting curtain reaches down into the layer.

The head distribution also illustrates that from the reservoir flow passes the insoluble layer and emerges through this layer downstream. These few examples not only show the wide field of applications of our modelling but also show that it is necessary to understand the more simple standard scenarios for the interpretation of more complex geological situations.

6. Conclusion

We have presented a model of evolution of karstification under high hydraulic heads and unnaturally short pathways of flow from an input to an output in limestone and gypsum terranes. Such conditions exist at dam sites. But also other hydraulic structures, e.g. impounding water in cave systems by blocking the outflows (Milanović, 2000) present similar conditions.

In the model, we simulate the initial conductivity by a fracture network with average aperture widths of several 10^{-2} cm. This is highly idealised. Nevertheless, nets with fracture aperture widths of 0.02 cm with spacing of 10 m correspond to hydraulic conductivities of 8×10^{-7} m s^{-1}, which is not unrealistic in karst. All our model runs show that under such conditions, large dam sites exhibit increasing leakage rates within their lifetimes. More complex geological setting can be incorporated into the model such as open phreatic or vadose cave conduits beneath the dam. It is also possible to model stratigraphic layers of the rock with varying properties with respect to hydraulic conductivity or dissolution kinetics. For instance, regions of low hydraulic conductivity, diverting flow paths to longer detours, will reduce leakage considerably and breakthrough times will be much longer. Regions of insoluble rock under favourable conditions can prevent breakthrough.

To model a real situation, detailed knowledge of the specific geological situation is needed. It is not a major problem to include this into the computer model where fracture widths, dissolution rate laws, lengths, etc. can be assigned to each fracture individually. Blockage of fractures by clays, either inflow or dissolutional widening, are also inhibitors for karstification. In the model runs discussed here, clay blockage is neglected. Therefore, a conclusion that karstification below dam sites in any case must lead to problems within their lifetimes cannot be regarded as generally valid. On the other hand, however, in view of the results presented here, one should not exclude the possibilities that enhanced karstification may lead to problems and this should be regarded in risk assessment.

The aim of this work is to draw attention to natural processes, which are not common in terranes of insoluble rocks, but could cause problems in karst regions.

References

Beek, W.J., Mutzall, K.M.K., 1975. Transport Phenomena. Wiley, New York.

Breznik, M., 1998. Storage Reservoirs and Deep Wells in Karst Regions. A.A. Balkema, Rotterdam.

Buhmann, D., Dreybrodt, W., 1985a. The kinetics of calcite dissolution and precipitation in geologically relevant situations of karst areas: 1. Open system. Chem. Geol. 48, 189–211.

Buhmann, D., Dreybrodt, W., 1985b. The kinetics of calcite dissolution and precipitation in geologically relevant situations of karst areas: 2. Closed system. Chem. Geol. 53, 109–124.

Dreybrodt, W., 1988. Processes in karst systems—physics, chemistry and geology. Springer Series in Physical Environments, vol. 4. Springer, Berlin. 188 pp.

Dreybrodt, W., 1990. The role of dissolution kinetics in the development of karstification in limestone: a model simulation of karst evolution. J. Geol. 98, 639–655.

Dreybrodt, W., 1992. Dynamics of karstification: a model applied to hydraulic structures in karst terranes. Appl. Hydrogeol. 1, 20–32.

Dreybrodt, W., 1996. Principles of early development of karst conduits under natural and man-made conditions revealed by mathematical analysis of numerical models. Water Resour. Res. 32, 2923–2935.

Dreybrodt, W., Buhmann, D., 1991. A mass transfer model for dissolution and precipitation of calcite from solutions in turbulent motion. Chem. Geol. 90, 107–122.

Dreybrodt, W., Eisenlohr, L., 2000. Limestone dissolution rates in karst environments. In: Klimchouk, A., Ford, D.C., Palmer, A.N., Dreybrodt, W. (Eds.), Speleogenesis: Evolution of Karst Aquifers. Nat. Speleol. Soc., USA, pp. 136–148.

Dreybrodt, W., Gabrovšek, F., 2000. Dynamics of the evolution of a single karst conduit. In: Klimchouk, A., Ford, D.C., Palmer, A.N., Dreybrodt, W. (Eds.), Speleogenesis: Evolution of Karst Aquifers. Nat. Speleol. Soc., USA, pp. 184–193.

Dreybrodt, W., Siemers, J., 2000. Cave evolution on two-dimensional networks of primary fractures in limestone. In: Klimchouk, A., Ford, D.C., Palmer, A.N., Dreybrodt, W. (Eds.), Speleogenesis: Evolution of Karst Aquifers. Nat. Speleol. Soc., USA, pp. 201–211.

Dreybrodt, W., Lauckner, J., Zaihua, L., Svensson, U., Buhmann, D., 1996. The kinetics of the reaction $CO_2 + H_2O \rightarrow H^+ + HCO_3^-$ as one of the rate limiting steps for the dissolution of calcite in the system $H_2O-CO_2-CaCO_3$. Geochim. Cosmochim. Acta 60, 3375–3381.

Dreybrodt, W., Romanov, D., Gabrovšek, F., 2001. Karstification below dam sites: a model of increasing leakage. In: Beck, B.F., Herring, J.G. (Eds.), Geotechnical and Environmental Applications of Karst Geology and Hydrology: Proceedings of the 8th Multidisciplinary Conference on Sinkholes and the Engineering and Environmental Impacts of Karsts, Louisville, Kentucky. Balkema, pp. 131–137.

Eisenlohr, L., Meteva, K., Gabrovšek, F., Dreybrodt, W., 1999. The inhibiting action of intrinsic impurities in natural calcium carbonate minerals to their dissolution kinetics in aqueous H_2O-CO_2 solutions. Geochim. Cosmochim. Acta 63, 989–1002.

Ford, D.C., Williams, P.W., 1989. Karst Geomorphology and Hydrology. Unwin Hyman, London.

Gabrovšek, F., 2000. Evolution of Early Karst Aquifers: From Simple Principles to Complex Models. Zalozba ZRC, Ljubljana, Slovenia. 150 pp.

Gale, J.E., 1987. Comparison of couplet fracture deformation and fluid flow models with direct measurement of fracture pore structure and stress-flow properties. Proceedings of the 28th U. S. Symposium of Rock Mechanics, Tucson, Arizona, 1987, p. 1213.

Groves, C.G., Howard, A.D., 1994. Early development of karst systems. 1. Preferential flow path enlargement under laminar flow. Water Resour. Res. 30, 2837–2846.

Howard, A.D., Groves, C.G., 1995. Early development of karst systems 2. Turbulent flow. Water Resour. Res. 31, 19–26.

Incropera, F.P., Dewitt, D.P., 1996. Fundamentals of Heat and Mass Transfer. Wiley, New York. 889 pp.

James, A.N., 1992. Soluble materials in civil engineering. Ellis Horwood Series in Civil Engineering. Ellis Horwood, Chichester, England. 434 pp.

Jeschke, A.A., Vosbeck, K., Dreybrodt, W., 2001. Surface controlled dissolution rates in aqueous solutions exhibit nonlinear dissolution kinetics. Geochim. Cosmochim. Acta 65, 13–20.

Klimchouk, A., Ford, D.C., Palmer, A.N., Dreybrodt, W. (Eds.), 2000. Speleogenesis: Evolution of Karst Aquifers. Nat. Speleol. Soc., USA. 444 pp.

Lee, C., Farmer, I., 1993. Fluid Flow in Discontinuous Rocks. Chapman & Hall, London.

Liu, Z., Dreybrodt, W., 1997. Dissolution kinetics of calcium carbonate minerals in H_2O-CO_2 solutions in turbulent flow: the role of the diffusion boundary layer and the slow reaction $H_2O + CO_2 \Leftrightarrow H^+ + HCO_3^-$. Geochim. Cosmochim. Acta 61, 2879–2889.

Milanović, P.T., 1981. Karst Hydrogeology. Water Resources Publication, Littleton, USA.

Milanović, P.T., 2000. Geological Engineering in Karst. Zebra Publishing, Belgrade, Yugoslavia.

Palmer, A.N., 1988. Solutional enlargement of openings in the vicinity of hydraulic structures in karst regions. 2nd Conference on Environmental Problems in Karst Terranes and Their Solutions. Assoc. of Groundwater Scientists and Engineers Proceedings, USA, pp. 3–15.

Palmer, A.N., 1991. The origin and morphology of limestone caves. Geol. Soc. Amer. Bull. 103, 1–21.

Press, W.F., Teukolsky, S.A., Vetterling, W.T., Flannery, B.P., 1992. Numerical Recipes in C: The Art of Scientific Computing. Cambridge Univ. Press.

Siemers, J., Dreybrodt, W., 1998. Early development of karst aquifers on percolation networks of fractures in limestone. Water Resour. Res. 34, 409–419.

Steward, D.E., Leyk, Z., 1994. Meschach: The Matrix Computation in C: Proceedings of the Centre For Mathematics And Its Applications, vol. 32. The Australian National University, Canberra, Australia.

Svensson, U., Dreybrodt, W., 1992. Dissolution kinetics of natural calcite minerals in CO_2–water systems approaching calcite equilibrium. Chem. Geol. 100, 129–145.

Uromeihy, A., 2000. The Kar Dam: an example of infrastructural development in a geologically active karstic region. J. Asian Earth Sci. 18, 25–31.

White, W.B., 1988. Geomorphology and Hydrology of Karst Terrains. Oxford Univ. Press, New York.